# Adherence to the conservation of momentum to elucidate membrane transporter mechanisms.

Briony A Yorke (1) & Helen M Ginn* (2,3)

(1) School of Chemistry, University of Leeds, Woodhouse Lane, Leeds, LS2 9JT, United Kingdom; (2) Center for Free-Electron Laser Science CFEL, Deutsches Elektronen-Synchrotron DESY, Notkestr. 85, 22607 Hamburg, Germany. (3) Institute for Nanostructure and Solid State Physics; University of Hamburg; Hamburg 22761, Germany; Corresponding author's email: helen.ginn@cfel.de;

## 1 Abstract

The conformational landscape of proteins and associated dynamics is an essential component of function. Diverse conformations of highly populated metastable states are well-studied, but transitions between these states are rare, fleeting events. Neither molecular dynamics simulations nor experimental methods provide information about these. To address this conundrum, we present a computationally inexpensive algorithm, "cold-inbetweening", which generates trajectories in torsion angle space. This minimises the overall kinetic energy needed to complete a transition between experimentally determined end-states. We use this method to provide mechanistic insight into three transporter superfamilies. This method allows interrogation of structural transitions, provides unique insights into coupled motion and hypotheses of action. The alternate access model of operation [1] is ubiquitous among many superfamilies of membrane transporters [2]. The model proposes that outward and inward pore opening is mutually exclusive, allowing ligand translocation but preventing damage from free solvent flow. Here, we study DraNramp (MntH) from *Deinococcus radiodurians* [3], MalT (bcMalT) from *Bacillus cereus* [4], and MATE (PfMATE) from *Pyrococcus furiosus* [5]. In MalT, the trajectory demonstrates elevator transport through unwinding of a supporter arm helix, maintaining the necessary and sufficient space to transport maltose. In DraNramp, this trajectory exhibited outward-gate closure prior to inward-gate opening, suggesting that the timing of gate closure is an inherent property of the protein architecture. In the MATE transporter, switching conformation involves the rewinding of an extended N-terminal helix. We suggest that the necessary motions to avoid steric backbone clashes forces this helix to plug the cavernous ligand-binding site during the conformational change. We propose helix unwinding as a general structural mechanism in membrane

transporter function due to ease of helix register slippage in the lipid bilayer.

# 2 Main

The protein conformational landscape has been identified as a cornerstone of understanding for protein function. However, due to the difficulty in observing or simulating large conformational transitions, there is a need for computational calculation of trajectories, for which previous efforts [6–10] have either not stood the test of time or are considered an aesthetical rather than analytical tool [11]. The way to and from these end-points remain surprisingly unanalysed. However, it is clear that the motion must be strongly influenced by the protein scaffold. The term "inbetweening" refers to a traditional method in animation for filling in the gaps between temporally sparse keyframes according to a protocol defined by physically plausible motions. Here, we apply this concept to protein dynamics by smoothly varying torsion angles using prior knowledge of the start and end structure [12]. We refer to this as "cold" inbetweening because we deliberately omit the model of Brownian motion.

The algorithm assumes regularised bond lengths, angles and optimised torsion angles [13] of both structures. Trajectories are determined by only allowing variation of torsion angles. Each pair of atoms has a starting and ending inter-atomic distance. A linear glidepath for these distances during the trajectory would minimise energy of the transition by conserving momentum and energy (Fig. 1A). However, this is not fully achievable due to the constraints imposed by limited freedom of motion in torsion angle space. Therefore, the torsion angles are adjusted to minimise the differences between the actual inter-atomic distances and their ideal glidepaths (Fig. 1B). Initially, torsion angles take a linear course between values from the start and end structure. Harmonic perturbations are added with refinable amplitudes to minimise deviation from the glidepaths (early-stage refinement). Residual clashes in sidechains are then resolved by minimising a combined energy term (late-stage refinement, see Methods).

## 2.1 Analysis of alternate access mechanisms.

The EIIC domain of the MalT transporter is purported to act by an elevator subcategory of alternate access. In elevator mechanisms, the ligand binds in a substrate-binding cavity. The protein-ligand interface moves as a rigid body, closing the outward gate prior to opening of the inward gate (PDB codes 6bvg and 5iws respectively). The contact points with the substrate remain largely unchanged during the transition [14]. The structure of this protein has been solved inwan outward- and inward-open conformation [4]. This was the simplest rearrangement in our study and we use this to demonstrate some characteristics of the method. We show the cold-inbetweened path in Fig. 1C. Use of harmonic

adjustments allows backbone atoms to follow near-perfect straight lines, despite moving by circular rotation around bonds. The ability to create straight lines out of combined rotations is conceptually similar to Fourier series summations of harmonics. Sidechains, often undergoing much larger motions than the backbone, often take more curvaceous routes due to restrictions of that movement around a limited number of bonds (Fig. 1D-F).

The full path shows the coupled winding of helix AH2 to become an extension of TM5, and a subsequent collapse of the angle between AH2 and TM6 (Extended Data Movie 1). Despite the method not explicitly modelling a ligand, we found that it is nevertheless suitable to maintaining the binding-cavity (Fig. 2A). This is because the starting and ending pairwise distances between atoms encode the size of the ligand-binding cavity, and there is no term in the target function which would lead to its collapse. Two residues V20 and V353 also appear to act as a gate, closing the maltose molecule off from the solvent during transit (Figure 2B,C). The cavity is also maintained by miniature unwinding events in helix TM1, which forms one of the three walls of the elevator (Extended Data Movie 1).

We applied the algorithm to less straightforward rearrangements. Mutations of human NRAMP proteins lead to immune deficiency and anaemia. However, model systems are more tractable [15, 16]. DraNramp is a bacterial homologue of human NRAMP proteins from *Deinococcus radiodurians* and a member of the ubiquitous LeuT superfamily. Mutations of NRAMP proteins lead to immune deficiency and anaemia. DraNramp transports manganese and other heavy metal ions from outward- to inward-facing sides of the membrane. Backflow of Mn(II) back down its concentration gradient during transport must be avoided. The first structure of DraNramp naturally crystallised in the inward-open form [3]. By introducing steric bulk in the outward-gate (G223W), DraNramp was crystallised in an outward-open form [17]. This mutation also impaired metal transport and prevented NEM modification of an inward-gate reporter site (A53C), demonstrating inward-gate closure does not occur if the outward gate is forced open [17]. This therefore supports the alternate access mechanism. LeuT fold proteins are purported to work by a rocking-bundle subcategory of alternate access [18, 19]. The binding site is enclosed between two rigid bodies, and is the fulcrum around which one of the rigid bodies rotates, thereby alternating access between the two sides. However, for all LeuT transporters, direct visualisation of the transition from inward- to outward-facing structures has, as for most large-scale conformational changes, been so far unattainable. The nature of transitions is highly sought after [20], including in DraNramp: "TM6b may ... move significantly itself in an as-yet-uncaptured conformational state" [21], "[TM6b] may undergo motions not yet captured in the available crystal structures" [22], "[sidechain] carbonyls both coordinating the metal substrate in an as-yet-uncaptured

intermediate state" [17]. Many solved structures of DraNramp have unmodelled loops. As a continuous chain of torsion angles is required for cold-inbetweening, we chose the fully-modelled Mn(II)-bound outward-open and inward-open conformations as end-points (PDBs 8e6n and 8e6i respectively) [23]. To preserve the original sequence, A230 was mutated to wildtype methionine presenting the rotamer from the discontinuous apo- inward-open structure (PDB 6d9w) [3]. We omitted the inward-occluded structure as it was unclear to what extent the G45R mutation was distorting the otherwise untethered TM1a helix.

In our pathway, a rapid and consistent contraction of TM10 and TM6a against TM1b closes off access to the ligand-binding site from the outward vestibule (Fig. 3A, Extended Data Movie 2). We monitor this using the area between the C$\alpha$ atoms of G58, A227 and Q378 (outward triangle), which steadily collapses (Fig. 3B). The inward-facing vestibule is opened by expansion of a gap between TM1a, TM6b and TM8. The inward triangle for the inward-facing vestibule encompasses C$\alpha$ atoms of S327, V233 and A53. In Fig. 3A, A53 rapidly moves away from the ligand-binding site through unwinding of the TM1a-b kinked region. However, this produces a shearing motion of TM1a against TM6b and TM8 in the first half of the pathway, which results in no overall change in the area of the outward triangle. It is only at the 50% mark that inward gate-opening picks up pace to allow solvent access to the ligand-binding site (Fig. 3C). This therefore supports and provides mechanistic details on the rocker-bundle mechanism. The pathway was heavily influenced by constraints on the substantial rearrangement of the TM6b-TM7 linker. Here, I245 could either flip clockwise or anti-clockwise by 180 ° to the other side of the backbone. Q246 must complete a counter turn either 90 ° in one direction or 270 ° in the other (Extended Data Movie 2). One of the two residues needs to turn through the interior of the protein while the other must turn towards the solvent, but only Q246 was able to achieve this without substantial, unresolvable clashes on the loop interior. Accommodation of the 270° turn led to a substantial mid-trajectory displacement of TM6b. TM6b moves 1.2 Å out of alignment mid-trajectory (Extended Data Fig. SS1). This suggests the mechanical hypothesis supports previous NEM-labelling data indicating TM6b moves substantially during conformational switching [21].

Finally, we examined a member of the MOP superfamily, the multidrug and toxic compound extrusion (MATE) transporter [24], often conferring resistance to antibiotics in bacteria. MATE from *Pyrococcus furiosus* has a large 4300 Å$^3$ cavity. Here, the inward-open and outward-open structures [5] differ by a dramatic rewinding of the central portion of the TM1 helix. Firstly, we checked Ramachandran outliers in the unwound structure: a peptide flip of G30 was found to fix a Ramachandran outlier in the inward-open conformation, which fit the density equally well. Other Ramachandran

outliers were favoured in their fit to the density and considered to be realistic in light of the dynamics in this region. The helix, in its unwound state, bridges the larger gap between the N-terminal domain and C-terminal domain; the fully-wound helix is also able to bridge the narrower gap in the outward-open state. One pertinent question is what combination of bond rotation directions allows the helix to rewind (or unwind) without causing steric clashes? By testing several combinations, we found a solution involving a mid-trajectory development and resolution of a kink in the middle of the helix (Fig. 4A, Extended Data Movie 3), which did not clash internally or with the rest of the protein (so-called "kinked winding"). This, however, protruded far from the helical axis. We initially attempted a direct recoiling of the extended helix, in order to minimise off-axis motion and thereby conserve momentum (so-called "straight winding", Fig. 4B). However, we found this would be highly energetically unfavourable due to a close carbonyl-carbonyl clash in adjacent residues (M27 and M28) on the backbone. It also led to a 270° rotation of the N-terminal section of TM1 around its axis. However, the kinked winding alternative has a more simple 180° shift of this region, which is a more achievable helix register slippage. We also note that at 95% progression through the kinked winding trajectory, the r.m.s.d. of $C_\alpha$ atoms of TM1 reaches a minimum against the bent conformation [25], whereas no mid-trajectory agreement of the straight winding path has a smaller r.m.s.d. than the end-point, strongly suggesting straight winding is not the mechanism by which the alternate access model operates. The kinked winding protrusion extends into the cavity mid-trajectory and thereby blocks solvent access to the cavity (Fig. 4C) which does not occur for straight winding (Figure 4D). We also checked for overlap of the kinked helix with ligand- and inhibitor-bound structures previously determined [25], and found that overlap with the ligand was insubstantial compared to that of the inhibitors (Extended Data Fig. S2).

## 3 Discussion

Here we show that cold-inbetweening can be used to estimate the feasibility of particular transitions and their consequences. Although in reality Brownian motion is the only route by which molecular dynamics can escape local energy minima, cold-inbetweening reduces the pathway to the core essential requirements of a transition for trusted end-points, thereby complementing the experimental determination of structures and simulations using the heat-driven engine of molecular dynamics simulations (MD). The omission of Brownian motion precludes direct comparison to the results of MD, and we do not assign a timescale to the trajectory. We show that cold-inbetweening preserves ligand-binding states due to their inclusion in the start and end models even without explicitly modelling an energy term for electrostatics and solvent reorganisation. In cases where there are crucial imperfections in

the fiducial end-points, these are imprinted on the trajectory and this method then often fails to find a low-energy route when applied to poorly modelled proteins with an unusually high proportion of Ramachandran outliers. This helps to prevent inaccurate conclusions being drawn from poorly modelled protein structures. However, in cases where structural data is available [26], we show that is it possible to improve the model and rectify true outliers prior to calculating the trajectory as applied here for MATE.

We note that in the three cases presented here, helix winding and unwinding is a common feature, as has been previously noted [19]. By cold-inbetweening the trajectory of the transitions, we can generate testable hypotheses as to how helix winding or unwinding may contribute to the protein's function. We suggest this mechanism is especially prominent in membrane proteins due to their lipid environment. In globular proteins, the first hydration shell surrounding the protein may provide additional enthalpic contributions to the energy barrier which must be overcome in order to allow a helix register to slip. It is conceivable therefore, that evolution would need to sample multiple mutations, on both the internal and external faces of the helix, in order to explore the fitness landscape in globular proteins. A fitness landscape requiring multiple mutations to progress function is rugged and hard to evolve [27]. The relative abundance of helix register slippage in membrane proteins may reflect the fact that fewer mutations are required as the external contact environments of transmembrane helices are towards less-ordered lipid tails, and therefore largely permissive. This may smoothen the fitness landscape explored by evolution to fine-tune these transitions, thereby making this a commonly exploited mechanism of action across membrane transporters. Cold-inbetweening addresses the untapped potential of information content in protein structural models to alter our way of thinking about evolution of transitions across the functional energy landscape.

### 3.1 Code availability.

The code for performing the cold-inbetweening is included in git commit 9da67bd of the RoPE software (https://github.com/helenginn/rope).

### 3.2 Data availability.

Ensemble models of the three transitions are included in the Extended Data.

# 4 Methods

## 4.1 Construction of parameter set.

The set of torsion angles refers to all torsion angles in a protein required to recalculate the protein's conformation. Each torsion angle varies as a function of $p$, which varies from 0 to 1 along the trajectory. The starting and ending structures of the protein are fixed. At $p = 0$, each torsion angle $t_i$ in the structure is defined to have the starting value $\theta_i^0$, and at $p = 1$, the ending value $\theta_i^1$. Each of the $t_i$ values for $i = 0 \ldots n$ is a linear sum of terms as a function of $p$. The first of these terms (order 0) is a linear interpolation as in Eq. 1 and has no parameters.

$$t_i^0(p) = \theta_i^0 + p(\theta_i^1 - \theta_i^0) \tag{1}$$

Additional terms are defined for the maximum order 3. $f_n$ for each $n$ is an amplitude and a refineable parameter, for which the default value is zero.

$$t_i^n(p) = f_n sin(np\pi) \text{ where } n = 1, 2, 3 \tag{2}$$

These are combined to produce an interpolation for each torsion angle with 3 refineable parameters,

$$t_i = t_i^0 + \sum_{n=0}^{3} t_i^n \tag{3}$$

## 4.2 Torsion angle direction choice.

For each torsion angle, the direction of clockwise or anticlockwise must be chosen, which is not necessarily evident from the start or end states. Torsion angles which differ by no more than 30° between start and end state are considered to move 30° rather than 330°. For all other torsion angles, an algorithm is employed to choose the more appropriate direction within the context of the rest of the molecule.

Each atom has a starting position, $a_i^0$, and an ending position $a_i^1$. At a position $p$ along the trajectory, an atom has a linearly interpolated position $a_i^p$:

$$a_i^p = a_i^0 + p(a_i^1 - a_i^0) \tag{4}$$

Sets of four atoms associated with each torsion angle were assigned consecutive values of $a_i^p$ for values of $p = 0, 0.1, 0.2 \ldots\ldots 1.0$. For the first iteration, a reference torsion angle was calculated from these sets of four atoms. For subsequent iterations, iteration $n$, an updated torsion angle was similarly

calculated, and either -360, 0 or 360 was added in order to minimise the difference with the reference torsion angle from iteration $n-1$. This torsion angle is then carried through for the next calculation for iteration $n+1$. The final torsion angle for $p = 1.0$ is taken to indicate the direction of travel for this atom.

### 4.3 Construction of early-stage target function.

Each atom has a starting position and ending position, which are a function of the set of torsion angles denoted by $\theta_i^0$ and $\theta_i^1$ over all $i$. This means that every pair of non-hydrogen atoms $i$ and $j$ have a calculable distance $d_p^{ij}$ for a given value of $p$, corresponding to an invariant beginning and ending distance at $p = 0$ and $p = 1$ respectively. Every pair of non-hydrogen atoms for which either $d_0^{ij}$ or $d_1^{ij}$ is below a fixed limit chosen to balance coverage of close contacts and computational efficiency (default value of 8 Å), and which are not covalently connected by three or fewer intervening bonds, is included in the early-stage target function.

$$J_{early} = \sqrt{\sum_i \sum_{j}^{j \neq i} \int_0^1 \omega_{ij} (d_q^{ij} - d_p^{ij})^2 \, dp} \quad \text{where} \quad d_q^{ij} = d_0^{ij} + p(d_1^{ij} - d_0^{ij}) \quad \text{and} \quad \omega_{ij} = (1 + d_p^{ij})^{-1} \tag{5}$$

This therefore forms a least squares target function between the target atomic distances or glide-paths $d_q^{ij}$, which are a linear interpolation with respect to $p$, and the calculated atomic distances $d_p^{ij}$ from the set of torsion angles for each value of $p$. In practice, $J_{early}$ is numerically integrated with a number of steps which is set to 12 by default. The $\omega_{ij}$ term upweights close contacts and helps escape overlapping protein backbones.

### 4.4 Construction of late-stage target function.

The late-stage target function measures Van der Waals contacts and torsion angle energies, calculated over the pairs of atoms (including hydrogens) similarly below a fixed limit, which may need to be larger than 8 Å depending on the scale of the conformational change.

$$J_{late} = J_{VdW} + J_{torsion} \tag{6}$$

$J_{VdW}$ consists of a discontinuous function measuring Van der Waals contacts above those expected from the target atomic distances using the two-term Lennard-Jones potential. This consists of a reference Van der Waals energy term $VdW_q(ij)$ for the interpolated distance, here $\epsilon$ is the potential

well depth and a measure of the interaction strength [28] and $\sigma^i$ is the van der Waals radius for atom $i$ multiplied by 0.75.

$$VdW_q(i,j) = 4\epsilon \left( \left( \frac{\sigma^i}{d_q^{ij}} \right)^{12} - \left( \frac{\sigma^i}{d_q^{ij}} \right)^{6} \right) \tag{7}$$

and a Van der Waals energy term $VdW_p(ij)$ for the calculated distance,

$$VdW_p(i,j) = 4\epsilon \left( \left( \frac{\sigma^i}{d_p^{ij}} \right)^{12} - \left( \frac{\sigma^i}{d_p^{ij}} \right)^{6} \right) \tag{8}$$

The $VdW_q$ term is often positive for hydrogens involved in hydrogen-bonding arrangements which should not necessarily be disturbed during the transition. Therefore, it is used as a threshold, so only the positive difference between $VdW_p$ and $VdW_q$ is considered.

$$VdW(i,j) = \begin{cases} VdW_p(ij) - VdW_q(ij) & \text{if } VdW_p(ij) > VdW_q(ij), \\ 0 & \text{otherwise.} \end{cases} \tag{9}$$

The Van der Waals component of the late-stage target function is calculated as follows.

$$J_{VdW} = \sum_i \sum_j^{j \neq i} VdW(i,j) \tag{10}$$

Consider the pair of atoms (A, B) for each bond in the structure. A torsion angle will connect four atoms in total. Each bond will be the centre of a number of related torsion angles. To generate a general torsion angle energy function which approximates the energies associated with eclipsed and staggered conformations, each torsion angle is considered in turn. We find the set of $n$ torsion angles centred on each bond. We then define the total torsion energy as a sum of each part,

$$J_{torsion} = \sum_{(A,B)} \sum_i^n E(t_i) \tag{11}$$

where $E(t_i)$ is the corresponding energy term of the $i$th torsion,

$$E(t_i) = z_T \left( 1 + \left( \frac{t_i}{\sigma} \right)^2 \right)^{-3} \quad \text{where} \quad z_T = \sqrt{z_{A'}^2 + z_{B'}^2} \tag{12}$$

In this bell-curve function, $z_{A'}$ and $z_{B'}$ are the atomic numbers of the terminal atoms of the torsion angle directly bonded to A and B, respectively. $\sigma$ denotes a bell curve width set to 60°.

$J_{late}$ is numerically integrated with the same 12 steps for path calculations, but with some adjustments in $J_{VdW}$. By nature of slicing of the pathway into intervals for numerical integration, sometimes

atoms may pass extremely close to each other, but the point of minimum distance falls in between two numerically integrated intervals. This would create a way in which a minimisation method can easily mis-fit, in conjunction with a rapidly-changing function like $J_{VdW}$. Therefore, a modification to this approach was taken: for an atom moving between intervals $n$ and $n+1$, $n-1$ and $n+2$ intervals were also used to generate a cubic spline in dimensions $x$, $y$, $z$ where the polynomial must pass through each of these atom positions. When comparing the trajectories of atoms $i$ and $j$, the minimum distance between these atoms between fractional values between $n$ and $n+1$ are found and this value is taken as the interval's partial sum towards the estimation of the total integral.

### 4.5 Minimisation protocols.

Minimisation against the $J_{early}$ term is carried out using the L-BFGS algorithm [29]. Minimisation is considered converged if there is less than a $10^{-3}$ change in the $J_{early}$ term after a L-BFGS refinement cycle. Gradient descent is carried out on $f_1$ for the set of all torsion angles until convergence is reached; then on $f_1, f_2$ until convergence is reached, and likewise for parameters $f_1, f_2, f_3$.

Minimisation against $J_{late}$ is carried out using the Nelder-Mead simplex descent algorithm [30]. As each sidechain is almost independent from the rest of the protein, barring other local sidechains, simplex descents are run for each sidechain concurrently. Parameters $f_1, f_2, f_3$ are refined for torsion angles which affect the sidechain and do not affect the main chain with a step size of $10°$. After this, residues are ranked in terms of descending $J_{late}$ terms, including all atoms contributing to that residue's side or main chain. This is followed by additional simplex descents for the five residues with the highest values of $J_{late}$ term. This two-stage process is repeated until the $J_{late}$ term does not decrease by more than 5%.

### 4.6 Manual adjustments of torsion angles.

Due to the subtlety of interactions between torsion angle directional choices, manual adjustment of a handful of parameters is required. Some backbone torsion angles must be manually adjustedwwhere many neighbouring bonds frequently exceed $90°$, as this is easily confusable with a $270°$ rotation in the opposite direction. These decision-making processes were aided by a GUI which visually displays atom trajectories and makes bond flipping and harmonic adjustment accessible to users. Harmonic adjustment was occasionally employed during Nelder-Mead minimisation in order to escape Van der Waals "tangled" side chains, which are trapped in local, but not global, minima due to crossed bonds.

## 4.7 Preparation of structures.

Structures were downloaded from PDB-REDO [31] to regularise the use of software used to refine structures. Structures were re-hydrogenated using *phenix.reduce*. These structures were prepared for cold-inbetweening using the RoPE software package [12] which optimises torsion angles to fit the experimentally determined model [13]. Before cold-inbetweening, to ensure the simplest transition, the torsion angles of 180°-symmetric side chains (phenylalanine, tyrosine, aspartate, glutamate, arginine) were made identical. Due to the lower resolution ($>$ 2.4 Å) of structures involved, this was also extended to residues which could be distinguished only at higher resolution (asparagine, glutamine, histidine). Cold-inbetweening is implemented in the RoPE software package.

## 4.8 Cavity calculations.

The calculation of the ligand cavity for EIIC domain of the MalT transporter was performed using the KVFinder web server [32]. The molecular surface of the protein was calculated using a 1.7 Å probe radius and the inaccessible regions were calculated using a 4 Å probe radius. The outer limits of the cavity were defined using a 2.4 Å removal distance. The cavity volume cutoff was set according to the molecular volume of maltose 241.54 $Å^3$. The molecular volume of maltose was calculated with MoloVol [33], using a carbon atom radius of 1.77 Å and oxygen radius of 1.50 Å, with a probe of 1.2 Å, grid resolution 0.2 Å and optimisation depth 4.

## References


[1] P. Mitchell, "A general theory of membrane transport from studies of bacteria," *Nature*, vol. 180, no. 4577, pp. 134–136, 1957.

[2] L. R. Forrest, Y.-W. Zhang, M. T. Jacobs, J. Gesmonde, L. Xie, B. H. Honig, and G. Rudnick, "Mechanism for alternating access in neurotransmitter transporters," *Proceedings of the National Academy of Sciences*, vol. 105, no. 30, pp. 10338–10343, 2008.

[3] A. T. Bozzi, L. B. Bane, W. A. Weihofen, A. Singharoy, E. R. Guillen, H. L. Ploegh, K. Schulten, and R. Gaudet, "Crystal structure and conformational change mechanism of a bacterial nramp-family divalent metal transporter," *Structure*, vol. 24, no. 12, pp. 2102–2114, 2016.

[4] J. G. McCoy, Z. Ren, V. Stanevich, J. Lee, S. Mitra, E. J. Levin, S. Poget, M. Quick, W. Im, and M. Zhou, "The structure of a sugar transporter of the glucose eiic superfamily provides insight into the elevator mechanism of membrane transport," *Structure*, vol. 24, no. 6, pp. 956–964, 2016.

[5] S. Zakrzewska, A. R. Mehdipour, V. N. Malviya, T. Nonaka, J. Koepke, C. Muenke, W. Hausner, G. Hummer, S. Safarian, and H. Michel, "Inward-facing conformation of a multidrug resistance mate family transporter," *Proceedings of the National Academy of Sciences*, vol. 116, no. 25, pp. 12275–12284, 2019.

[6] Y. Ye and A. Godzik, "Fatcat: a web server for flexible structure comparison and structure similarity searching," *Nucleic acids research*, vol. 32, no. suppl_2, pp. W582–W585, 2004.

[7] W. G. Krebs and M. Gerstein, "Survey and summary: The morph server: a standardized system for analyzing and visualizing macromolecular motions in a database framework," *Nucleic acids research*, vol. 28, no. 8, pp. 1665–1675, 2000.

[8] E. Lindahl, C. Azuara, P. Koehl, and M. Delarue, "Nomad-ref: visualization, deformation and refinement of macromolecular structures based on all-atom normal mode analysis," *Nucleic acids research*, vol. 34, no. suppl_2, pp. W52–W56, 2006.

[9] J. Franklin, P. Koehl, S. Doniach, and M. Delarue, "Minactionpath: maximum likelihood trajectory for large-scale structural transitions in a coarse-grained locally harmonic energy landscape," *Nucleic acids research*, vol. 35, no. suppl_2, pp. W477–W482, 2007.

[10] O. S. Smart, "A new method to calculate reaction paths for conformation transitions of large molecules," *Chemical physics letters*, vol. 222, no. 5, pp. 503–512, 1994.

[11] W. L. DeLano *et al.*, "Pymol: An open-source molecular graphics tool," *CCP4 Newsl. Protein Crystallogr*, vol. 40, no. 1, pp. 82–92, 2002.

[12] H. M. Ginn, "Torsion angles to map and visualize the conformational space of a protein," *Protein Science*, vol. 32, no. 4, p. e4608, 2023.

[13] "Vagabond: bond-based parametrization reduces overfitting for refinement of proteins," *Acta Crystallographica Section D: Structural Biology*, vol. 77, no. 4, pp. 424–437, 2021.

[14] A. A. Garaeva and D. J. Slotboom, "Elevator-type mechanisms of membrane transport," *Biochemical Society Transactions*, vol. 48, no. 3, pp. 1227–1241, 2020.

[15] I. A. Ehrnstorfer, E. R. Geertsma, E. Pardon, J. Steyaert, and R. Dutzler, "Crystal structure of a slc11 (nramp) transporter reveals the basis for transition-metal ion transport," *Nature Structural & Molecular Biology*, vol. 21, no. 11, pp. 990–996, 2014.

[16] I. A. Ehrnstorfer, C. Manatschal, F. M. Arnold, J. Laederach, and R. Dutzler, "Structural and mechanistic basis of proton-coupled metal ion transport in the slc11/nramp family," *Nature Communications*, vol. 8, no. 1, p. 14033, 2017.

[17] A. T. Bozzi, C. M. Zimanyi, J. M. Nicoludis, B. K. Lee, C. H. Zhang, and R. Gaudet, "Structures in multiple conformations reveal distinct transition metal and proton pathways in an nramp transporter," *Elife*, vol. 8, p. e41124, 2019.

[18] J. A. Licht, S. P. Berry, M. A. Gutierrez, and R. Gaudet, "They all rock: A systematic comparison of conformational movements in leut-fold transporters," *bioRxiv*, 2024.

[19] D. Drew and O. Boudker, "Ion and lipid orchestration of secondary active transport," *Nature*, vol. 626, no. 8001, pp. 963–974, 2024.

[20] M. Hirschi, Z. L. Johnson, and S.-Y. Lee, "Visualizing multistep elevator-like transitions of a nucleoside transporter," *Nature*, vol. 545, no. 7652, pp. 66–70, 2017.

[21] A. T. Bozzi, A. L. McCabe, B. C. Barnett, and R. Gaudet, "Transmembrane helix 6b links proton and metal release pathways and drives conformational change in an nramp-family transition metal transporter," *Journal of Biological Chemistry*, vol. 295, no. 5, pp. 1212–1224, 2020.

[22] A. T. Bozzi and R. Gaudet, "Molecular mechanism of nramp-family transition metal transport," *Journal of Molecular Biology*, vol. 433, no. 16, p. 166991, 2021.

[23] S. Ray, S. P. Berry, E. A. Wilson, C. H. Zhang, M. Shekhar, A. Singharoy, and R. Gaudet, "High-resolution structures with bound mn2+ and cd2+ map the metal import pathway in an nramp transporter," *Elife*, vol. 12, p. e84006, 2023.

[24] X. He, P. Szewczyk, A. Karyakin, M. Evin, W.-X. Hong, Q. Zhang, and G. Chang, "Structure of a cation-bound multidrug and toxic compound extrusion transporter," *Nature*, vol. 467, no. 7318, pp. 991–994, 2010.

[25] Y. Tanaka, C. J. Hipolito, A. D. Maturana, K. Ito, T. Kuroda, T. Higuchi, T. Katoh, H. E. Kato, M. Hattori, K. Kumazaki, *et al.*, "Structural basis for the drug extrusion mechanism by a mate multidrug transporter," *Nature*, vol. 496, no. 7444, pp. 247–251, 2013.

[26] R. P. Joosten and G. Vriend, "Pdb improvement starts with data deposition," *Science*, vol. 317, no. 5835, pp. 195–196, 2007.

[27] P. A. Romero and F. H. Arnold, "Exploring protein fitness landscapes by directed evolution," *Nature reviews Molecular cell biology*, vol. 10, no. 12, pp. 866–876, 2009.

[28] W. D. Cornell, P. Cieplak, C. I. Bayly, I. R. Gould, K. M. Merz, D. M. Ferguson, D. C. Spellmeyer, T. Fox, J. W. Caldwell, and P. A. Kollman, "A second generation force field for the simulation of proteins, nucleic acids, and organic molecules," *Journal of the American Chemical Society*, vol. 117, no. 19, pp. 5179–5197, 1995.

[29] D. C. Liu and J. Nocedal, "On the limited memory bfgs method for large scale optimization," *Mathematical programming*, vol. 45, no. 1, pp. 503–528, 1989.

[30] J. A. Nelder and R. Mead, "A simplex method for function minimization," *The computer journal*, vol. 7, no. 4, pp. 308–313, 1965.

[31] R. P. Joosten, J. Salzemann, V. Bloch, H. Stockinger, A.-C. Berglund, C. Blanchet, E. Bongcam-Rudloff, C. Combet, A. L. Da Costa, G. Deleage, *et al.*, "Pdb_redo: automated re-refinement of x-ray structure models in the pdb," *Applied Crystallography*, vol. 42, no. 3, pp. 376–384, 2009.

[32] J. V. Guerra, H. V. Ribeiro-Filho, J. G. Pereira, and P. S. Lopes-de Oliveira, "Kvfinder-web: a web-based application for detecting and characterizing biomolecular cavities," *Nucleic Acids Research*, vol. 51, no. W1, pp. W289–W297, 2023.

[33] J. B. Maglic and R. Lavendomme, "Molovol: an easy-to-use program for analyzing cavities, volumes and surface areas of chemical structures," *Journal of applied crystallography*, vol. 55, no. 4, pp. 1033–1044, 2022.

## 5 Acknowledgements

We thank David Stuart, Stephen McCarthy and Ilme Schlichting for comments on this paper and providing valuable feedback. H.M.G. is funded by the Helmholtz Association, grant VH-NG-19-02 (Helmholtz Young Investigator Group).

## 6 Author Contributions

B.A.Y. data analysis, co-wrote the paper. H.M.G. research conception, wrote the cold-inbetweening code, data analysis, co-wrote the paper.

## 7 Competing Interests

The authors declare no competing interests.

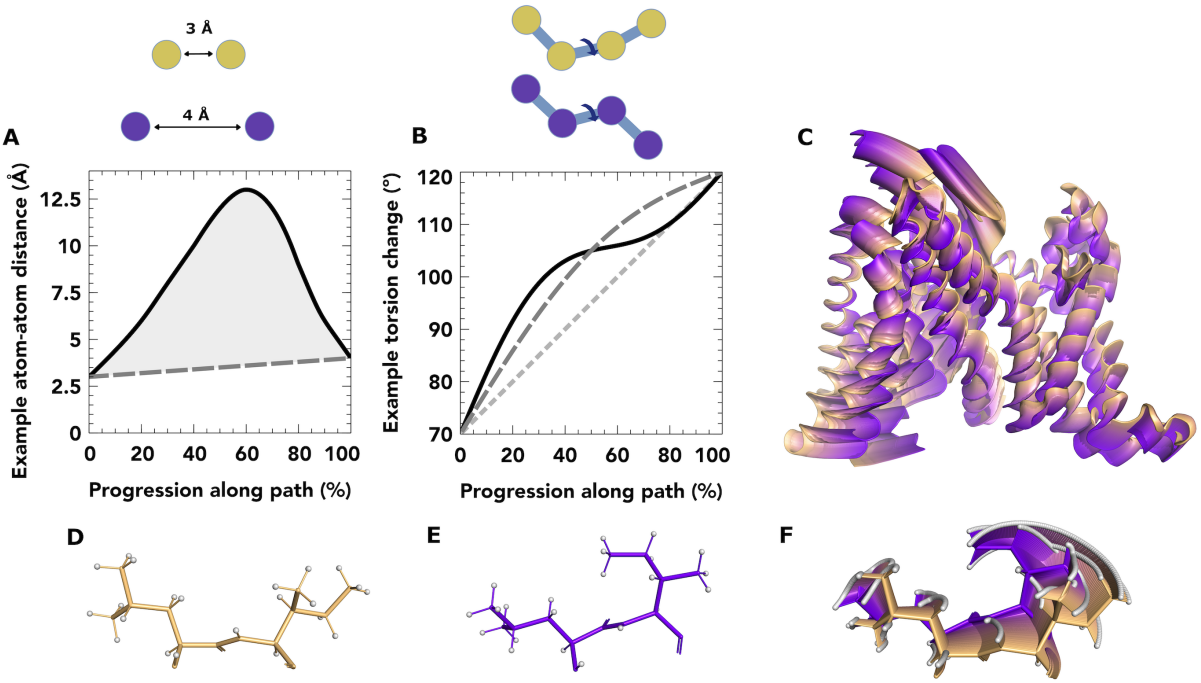


Fig. 1: (A) illustrative atom-atom distance term of momentum target function showing torsion angle-mediated distance (black solid), and target glidepath (dark grey dashed). Minimisation reduces shaded area. (B) torsion angle trajectories are parameters, starting from linear interpolation (light grey dotted), addition of a first-order harmonic (dark grey dashed) and second-order (black solid). Relative contributions of perturbations serve as parameters. (C) after refinement of MalT transporter path, overall motion rendering the entire pathway from outward-open (orange) to inward-open (purple) in 1% steps. (D-F) zoom-in of residues 385 and 386, showing (D) start-, (E) end-state and (F) all 1% steps superimposed. (C-F) figures generated in PyMOL [11].

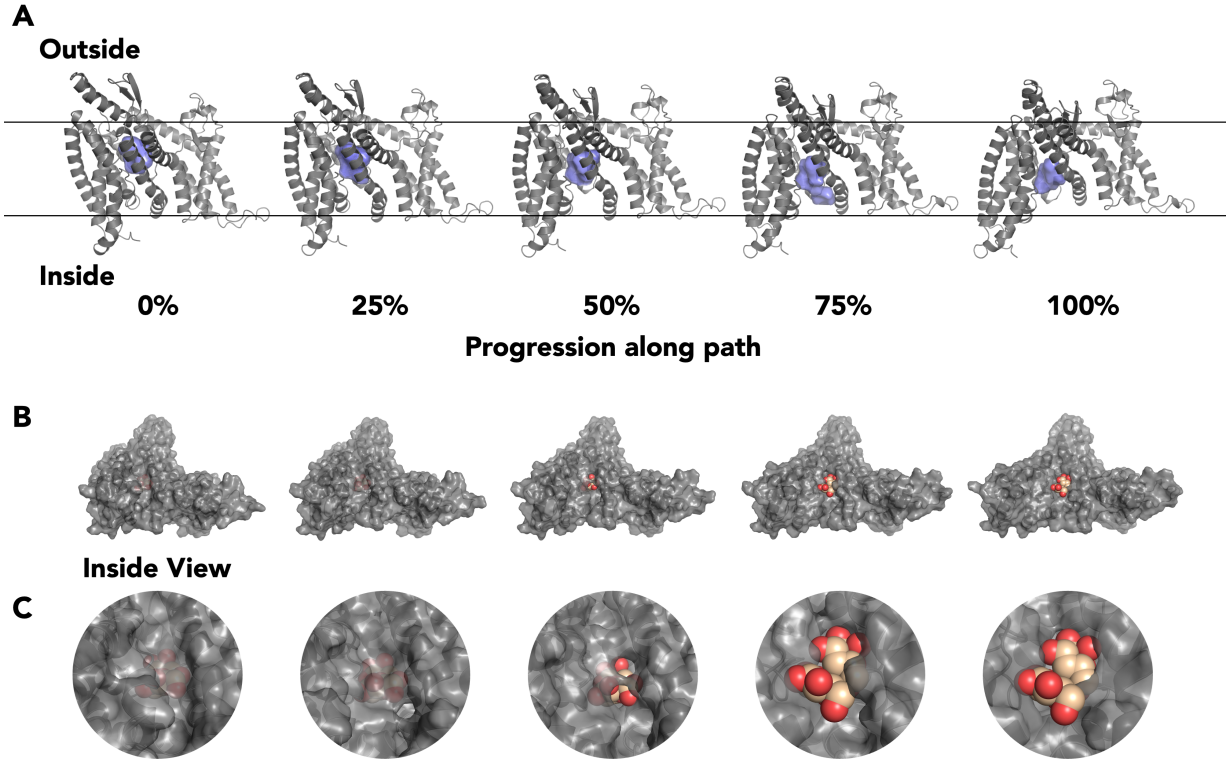


Fig. 2: (A) movements of the binding cavity in the EIIC domain of the MalT transporter, in 25% intervals along the trajectory with 0% and 100% corresponding to outward-open and inward-open respectively. In each figure the binding cavity, shown as a blue surface, was calculated using KVfinder [32]. (B) inside view of MalT showing movement of maltose (orange) in the binding cavity and opening of the inward pore. At 0% progression the maltose co-ordinates were taken directly from the outward open stucture (PDB 5iws), for progressive frames the maltose was manually translated to fit inside the cavities using PyMOL [11]. (C) Close-up of the inside pore opening of MalT and movement of maltose.

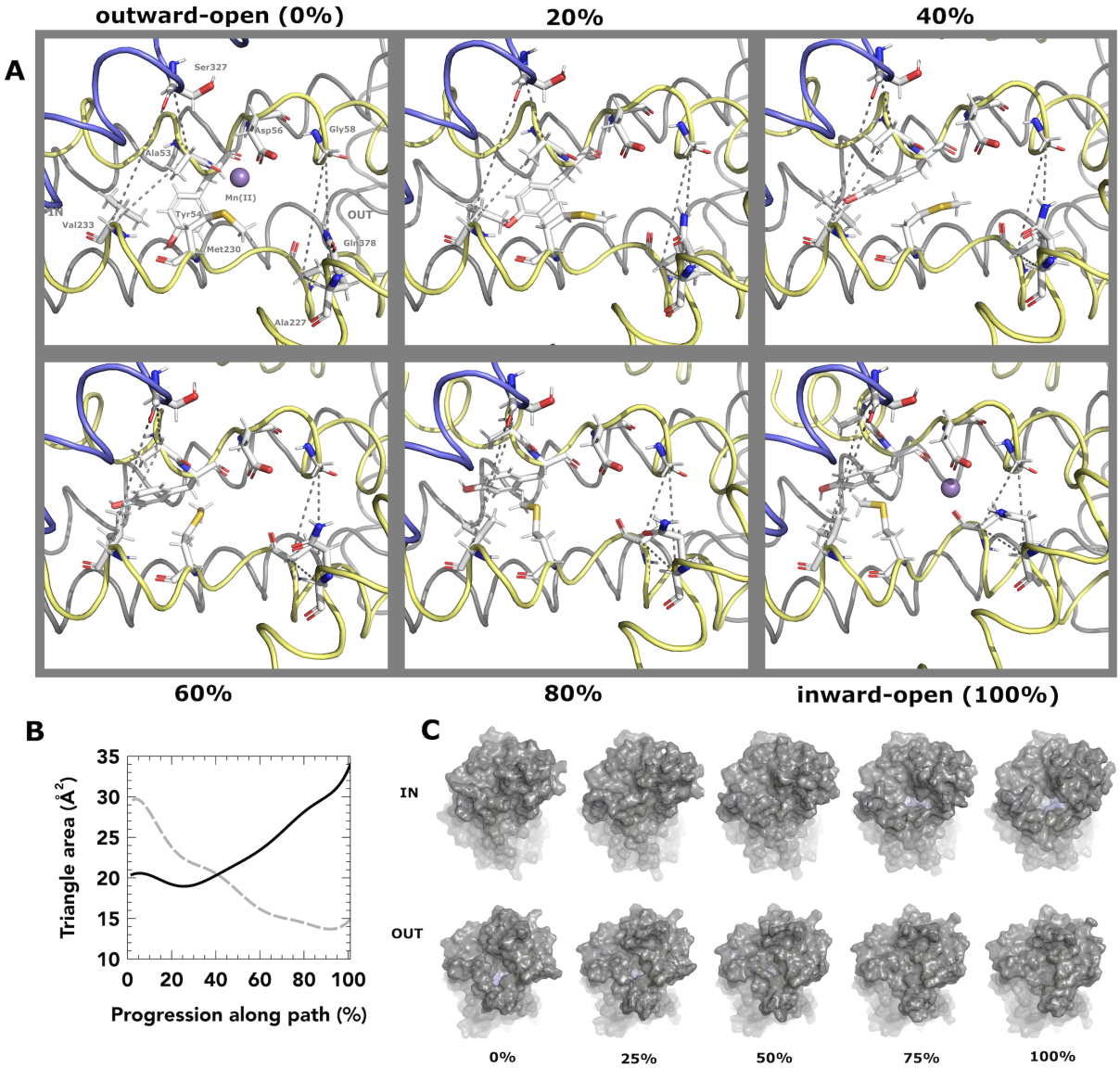


Fig. 3: (A) movements at the ligand-binding site (TM helices 3 and 8 removed for clarity) in 20% intervals along the trajectory, with 0% and 100% corresponding to outward-open and inward-open, respectively. In each figure, the left dotted triangle reports on the solvent accessibility to the inward gate, and the right dotted triangle reports on that of the outward gate. (B) area of inward triangle (black solid line) and outward triangle (grey dashed line) along path. (C) surface render from outward and inward sides for five points on path, with residues rendered as sticks in (A) coloured light blue.

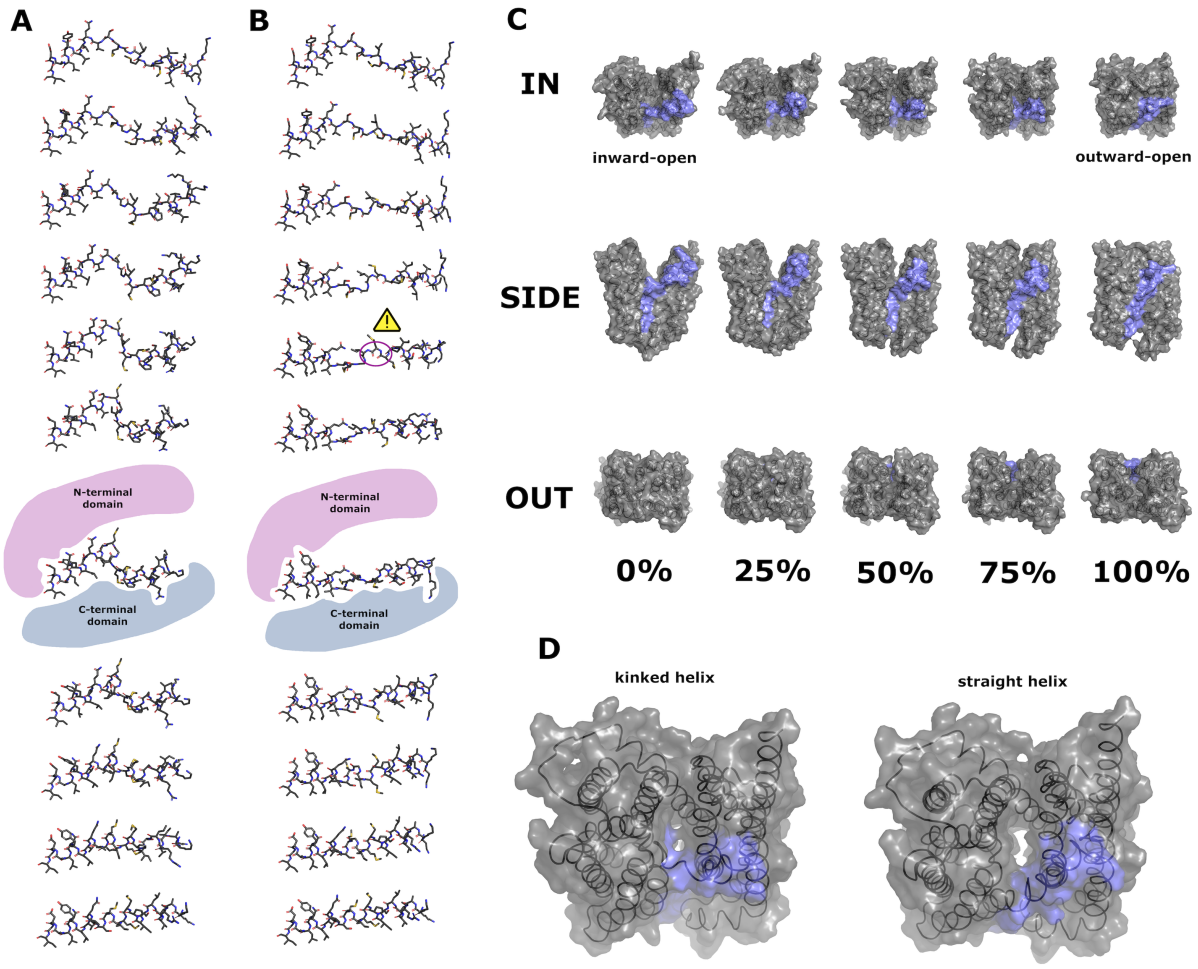


Fig. 4: (A) 10% increments in progression from 0% (top) to 100% (bottom) showing atomic trajectory of TM1 with torsion angle flips assigned as necessary to avoid backbone clashes ("kinked helix" trajectory). N-terminus is to the right. (B) similar increments in progression showing atomic trajectory of helix minimising out-of-axis motion ("straight helix" trajectory). Carbonyl clash on backbone highlighted with a warning sign. For (A) and (B) the 60% progression point is augmented by an illustration of relative positions of N-terminal and C-terminal domains. (C) view of kinked helix trajectory from the inward, side and outward views. TM1 residues 1-43 are marked in blue. (D) comparative views of kinked and straight helix trajectories at 70% trajectory, showing the aberrant opening of a solvent channel when all other protein motions with a straight helix trajectory are considered.

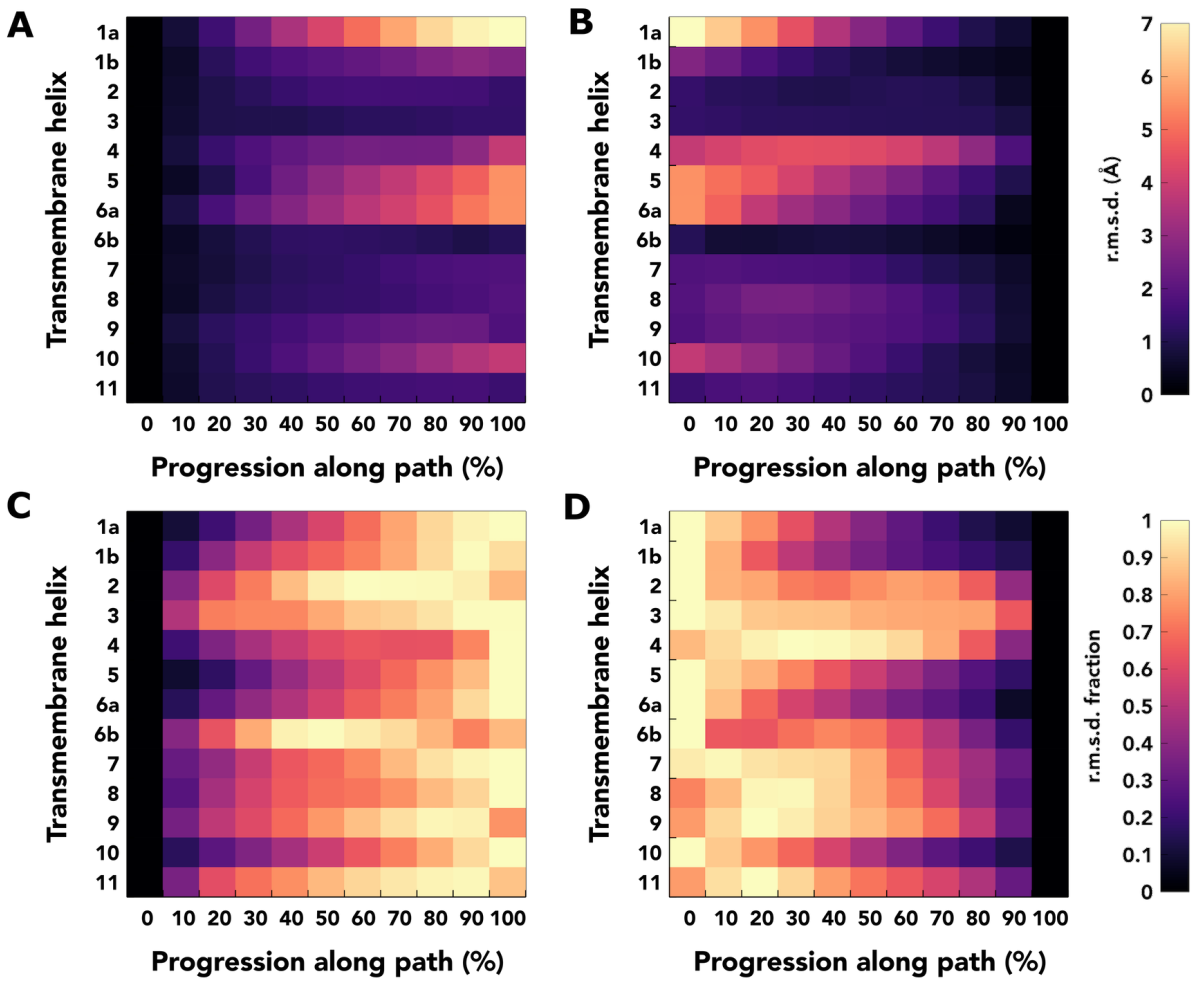


Extended Data Fig. S1: Helix alignments of mid-trajectory points along the pathway with the start and end points of the DraNramp cold-inbetweened pathway. (A, B) alignment in absolute r.m.s.d. against (A) 0% of trajectory and (B) 100% of trajectory. (C, D) alignment where each helix alignment is expressed as a fraction of the maximum r.m.s.d. for that helix, against (C) 0% trajectory and (D) 100% trajectory, respectively.

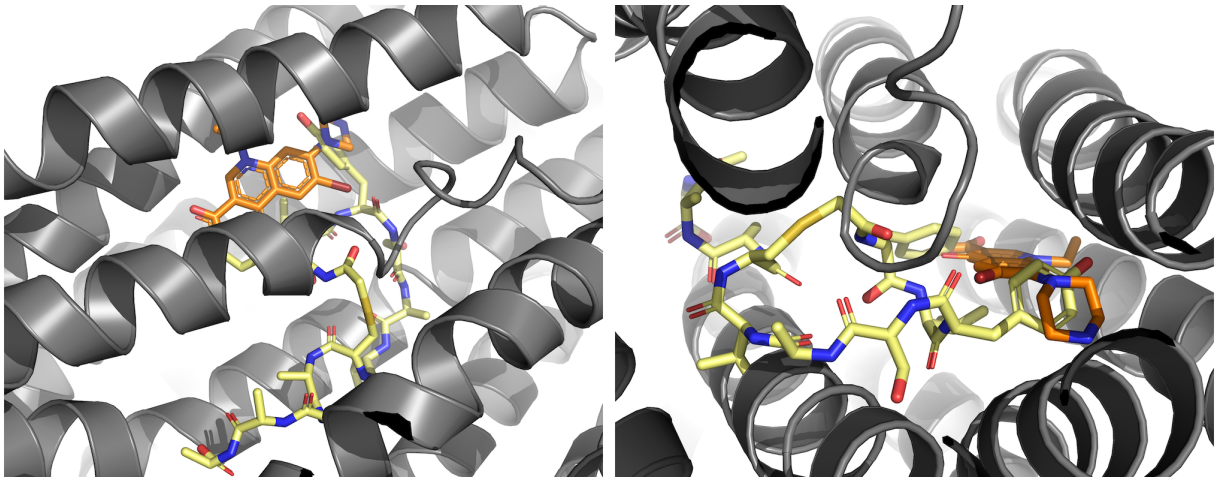

Extended Data Fig. S2: Two views of 70% progression (gray) through the MATE transition from inward- to outward-open, at the kinked TM1 unwinding position. Overlaid are the Br-NRF ligand-bound structure (orange) and the MaD5 inhibitor-bound structure (yellow) using all atoms in residues 165-185 for structure alignment (TM3, adjacent to ligand-binding site).